

CERN-TH 7291/94
 DFTT 22/94
 DF-UNICAL/94-15
 MS-TPI-94-6
 July 1994

Rough Interfaces Beyond the Gaussian Approximation

M. Caselle^a, R. Fiore^b, F. Gliozzi^a,
 M. Hasenbusch^c, K. Pinn^d and S. Vinti^a

^a *Dipartimento di Fisica Teorica dell'Università di Torino
 Istituto Nazionale di Fisica Nucleare, Sezione di Torino
 via P.Giuria 1, I-10125 Torino, Italy **

^b *Dipartimento di Fisica, Università della Calabria
 Istituto Nazionale di Fisica Nucleare, Gruppo collegato di Cosenza
 Rende, I-87030 Cosenza, Italy †*

^c *Theory Division, CERN
 CH-1211 Geneva 23, Switzerland ‡*

^d *Institut für Theoretische Physik I, Universität Münster
 Wilhelm-Klemm-Str. 9, D-48149 Münster, Germany §*

Abstract

We compare predictions of the Capillary Wave Model beyond its Gaussian approximation with Monte Carlo results for the energy gap and the surface energy of the 3D Ising model in the scaling region. Our study reveals that the finite size effects of these quantities are well described by the Capillary Wave Model, expanded to two-loop order (one order beyond the Gaussian approximation).

*e-mail: caselle, gliozzi, vinti @to.infn.it

†e-mail: fiore @fis.unical.it

‡e-mail: hasenbus @surya11.cern.ch

§e-mail: pinn @xtp139.uni-muenster.de

1 Introduction

Soft modes play an essential role in the description of *finite size effects* (FSEs) in the fluid interface's free energy (see for instance [1] and references therein). 3D spin systems offer a simple context where these effects appear and can be studied, e.g. by using numerical simulations to check theoretical predictions. It is well known that, between the roughening and the critical temperature of the 3D Ising model, interfaces are dominated by long wavelength fluctuations (i.e. they behave as *fluid* interfaces). Because of these fluctuations, a complete control on the description of interfaces, starting from the microscopic Hamiltonian, has not yet been reached in the rough phase. The usual approach consists in assuming an effective Hamiltonian describing the collective degrees of freedom.

An effective model widely used to describe a rough interface is the *capillary wave model* (CWM) [2]. In its simplest formulation one assumes an effective Hamiltonian proportional to the variation of the surface's area with respect to the classical solution. Because of its non-polynomial nature, until recently the CWM has been studied only in its quadratic approximation, the Hamiltonian being equivalent to a (massless) 2D Gaussian model. The CWM has been often identified with the Gaussian model. This model was shown to give a good description of several features of the interfaces of the 3D Ising model, like the logarithmic growth (as a function of the lattice size) of the interfacial width in the whole rough phase [3], and the FSEs (as a function of the shape of the lattice) of the free interface energy in the scaling region of the model [4].

The corrections that arise when passing from the classical approximation to the Gaussian one [5, 6, 4], (which we shall term from now on *one-loop* contributions), only depend on one adimensional parameter (namely on the asymmetry $u = L_2/L_1$ of the transverse sizes of the lattice) and on the boundary conditions. They reduce on symmetric lattices ($u = 1$) to the well known finite-size behaviour of the free energy [7, 8] in the large L limit

$$\frac{F}{k_B T} \propto \sigma L^2, \quad (1)$$

σ being the reduced interface tension.

As mentioned above, the CWM has been often identified with its Gaussian approximation. However, the full CWM is interesting in itself because of its simple geometrical meaning (see for instance Ref. [9] and references therein). Also, it coincides with the Nambu-Goto string action in a partic-

ular gauge (see the next section). The improvement of Monte Carlo simulations reached in the last years allows now to test the CWM beyond the Gaussian approximation. This is the aim of this paper, in which we investigate the presence of corrections to the pure Gaussian description of the free energy of a rough interface in the scaling region of the 3D Ising model.

A similar analysis was recently made in the context of the 3D three-state Potts model [10]. It was shown that higher order corrections to the Gaussian approximation of the CWM (from now on called *two-loop* contributions) give contributions to the functional form of the interface's free energy which can be exactly estimated.

The contributions to the interface free energy (i.e. vacuum diagrams on finite volumes) due to higher order expansion of the CWM Hamiltonian are finite and can be evaluated in a simple way [11]. In this paper we present evidence that the results are independent of the regularization used.

It turns out that the two-loop contributions do not depend only on the asymmetry parameter u but also on the adimensional expansion parameter proportional to the minimal area of the surface, namely $\sigma A \equiv \sigma L_1 L_2$. As a consequence and in contrast to what happens for the Gaussian model, even for symmetric ($L_1 = L_2 \equiv L$) lattices the finite-size behaviour of the free energy defined in Eq. (1) gets corrections proportional to $(\sigma L^2)^{-1}$ which are important in extracting the interface tension value using a fitting procedure. In this paper we discuss this picture for the Ising model, checking the theoretical prediction by means of Monte Carlo simulations and using very different techniques and algorithms.

Finally, let us remark that the 3D Ising model is related through duality to 3D Z_2 gauge theory. In particular the physics of interfaces is directly linked to the physics of their dual gauge observables, i.e. the Wilson loops, and, as a consequence, to the properties of the chromo-electric flux tube in the confining phase [12]. This means that all the results that we describe in this paper have a direct counterpart in the context of Lattice Gauge Theories, and could help to better understand the possible string-like descriptions of their infrared behaviour.

The paper is organized as follows: in Sec. 2 we review the model for rough interfaces near the continuum. In Sec. 3 we present an alternative derivation of the two-loop calculation given in Ref. [11]. In Sec. 4 we introduce and discuss the different observables and Monte Carlo techniques used to test the CWM. In Sec. 5 we analyze the numerical results.

2 The Models

2.1 The Ising Model

We consider the 3D Ising model on a regular cubic lattice of size L_1, L_2 in the x -, y -directions, where $L_2 \geq L_1$, and size t in the z -direction. In the x - and the y -direction periodic boundary conditions are imposed, while in the z -direction either periodic or anti-periodic boundary conditions are used, depending on the Monte Carlo method that is applied. The Hamiltonian is defined by

$$H = - \sum_{\langle ij \rangle} s_i s_j \quad , \quad (2)$$

where the sum is over all nearest-neighbour pairs $\langle ij \rangle$, and $s_i = \pm 1$. The corresponding partition function is

$$Z_I = \sum_{\{s_i = \pm 1\}} e^{-\beta H} \quad , \quad (3)$$

where $\beta = 1/(k_B T)$. The critical temperature of the model is estimated to be $\beta_c = 0.221652(3)$ [13]. The most precise estimate for the roughening coupling is $\beta_r = 0.4074(3)$ [14].

We study the model between the critical and the roughening temperature, namely in the region $\beta_r > \beta > \beta_c$.

While in infinite volume, for $\beta > \beta_c$, the system shows a spontaneous symmetry breaking, in finite volume this cannot occur, and interfaces appear, separating extended domains of different magnetization.

In particular, we will consider interfaces that are parallel to the $x - y$ plane and fluctuate freely in the third, orthogonal, z -direction. In section 4 we shall discuss how such interfaces can be generated in a Monte Carlo simulation.

Above the roughening temperature ($\beta_r > \beta > \beta_c$) the step free energy of the interface goes to zero. As a consequence the interface behaves essentially as a 2D critical system: it may be freely translated through the medium and the long-wavelength, transverse fluctuations in the interface position, i.e. capillary waves, have a small cost in energy (hence cannot be neglected in calculations). They can be viewed as the Goldstone modes associated with the spontaneous breaking of the transverse translational invariance [18]. To describe the interface free energy one is therefore forced to assume an effective model. On the other side, one has the advantage of choosing a Hamiltonian defined directly on the continuum to make analytical computations.

2.2 The Effective Model

We assume the effective Hamiltonian of the interface to be proportional to its area. Denoting by $x_i(\xi_1, \xi_2)$, $i = 1, 2, 3$, the coordinates of a point of the interface as functions of the parameters ξ_α , $\alpha = 1, 2$, with $0 \leq \xi_\alpha \leq 1$, we can write the area in the standard reparametrization invariant form,

$$\mathcal{A} = \int_0^1 d\xi_1 \int_0^1 d\xi_2 \sqrt{g} \ , \quad (4)$$

where $g = \det(g_{\alpha\beta})$, with

$$g_{\alpha\beta} = \frac{\partial x_i}{\partial \xi_\alpha} \frac{\partial x^i}{\partial \xi_\beta} \ . \quad (5)$$

A system with a Hamiltonian proportional to \mathcal{A} coincides with the Nambu–Goto model for the bosonic string. The corresponding quantum theory is anomalous: depending on the quantization method one finds either the breaking of rotational invariance or the appearance of interacting longitudinal modes (Liouville field). We are, however, interested in interfaces of very large size where these difficulties disappear and the rotational invariance is restored [19]; in the infrared limit the theory flows to the massless Gaussian model. In order to study the first perturbative correction to this limit it is convenient to assume that the main contribution to the interface free energy is given in this region by small and smooth deformations of the minimal surface (which is a flat torus of area $L_1 L_2$). More precisely, we assume that there are no foldings nor self-intersections nor overhangs¹. Under these conditions we can choose as parameters the two longitudinal coordinates $x = x_1$ and $y = x_2$, by putting $\xi_1 = x_1/L_1$ and $\xi_2 = x_2/L_2$; as a consequence, the transverse displacement x_3 of the surface becomes a single-valued function of them: $x_3 = \phi(x, y)$. In such a frame Eq. (4) can be written as

$$A[\phi] = \int_0^{L_1} dx \int_0^{L_2} dy \sqrt{1 + \left(\frac{\partial\phi}{\partial x}\right)^2 + \left(\frac{\partial\phi}{\partial y}\right)^2} \ . \quad (6)$$

¹ From the microscopic point of view this is not obvious *a priori*: in fact it has been observed that the interface at small scales is much more similar to a sponge than to a smooth surface [20, 21]. The strong linear correlation between the area and the genus of the surface (number of microscopic handles), together with the evidence that the partition function summed over all genera behaves like a smooth surface, has led to conjecture that a simple non-perturbative renormalization of the physical quantities associated to the surface occurs [21].

Using these notations, the free energy of a fluid interface can be described by

$$F = -k_B T \ln Z \quad (7)$$

$$Z = \lambda e^{-\sigma L_1 L_2} Z_q(\sigma, L_1, L_2) \quad (8)$$

$$Z_q = \int [D\phi] \exp\{-\mathcal{H}[\phi]\} \quad , \quad (9)$$

where λ is an undetermined constant within this approach. The reduced Hamiltonian \mathcal{H} is given by

$$\mathcal{H}[\phi] = \sigma (A[\phi] - L_1 L_2) \quad . \quad (10)$$

In words, $\mathcal{H}[\phi]$ is given by the change produced by the deformation ϕ in the interface's area, measured in units of the interface tension σ .²

One can then take into account the quantum contributions by expanding Eq. (10) in the natural adimensional parameter $(\sigma A)^{-1}$, $A = L_1 L_2$. The interface tension is the only dimensional parameter of this theory.

Coming back to the adimensional parameters $\xi_\alpha = x_\alpha/L_\alpha$, and putting $\phi' = \sqrt{\sigma}\phi$, the Hamiltonian can be written as

$$\mathcal{H}[\phi] = \sigma A \int_0^1 d\xi_1 \int_0^1 d\xi_2 \left[\sqrt{1 + \frac{1}{\sigma A} (\nabla\phi)^2} - 1 \right] \quad (11)$$

$$(\nabla\phi)^2 = u \left(\frac{\partial\phi}{\partial\xi_1} \right)^2 + \frac{1}{u} \left(\frac{\partial\phi}{\partial\xi_2} \right)^2 \quad , \quad (12)$$

where $u = L_2/L_1$, and the primes have been omitted. For $(\sigma A)^{-1} \rightarrow 0$, expanding up to the second order, one obtains

$$\mathcal{H}[\phi] = \mathcal{H}_g[\phi] - \frac{1}{8\sigma A} \mathcal{H}_p[\phi] + O((\sigma A)^{-2}) \quad (13)$$

$$\mathcal{H}_g[\phi] = \frac{1}{2} \int_0^1 d\xi_1 \int_0^1 d\xi_2 (\nabla\phi)^2 \quad (14)$$

$$\mathcal{H}_p[\phi] = \int_0^1 d\xi_1 \int_0^1 d\xi_2 ((\nabla\phi)^2)^2 \quad . \quad (15)$$

² Far from the scaling region, the interface tension σ in Eq. (10) should be replaced by the stiffness K . However, in the scaling region, as the bulk correlation length increases and the rotational invariance is restored, K approaches σ and for all the values of β that we studied the difference between them can be safely neglected [3].

Retaining only the quadratic term of Eq. (14) in the Hamiltonian (13), one obtains from Eq. (9) the one-loop contribution which constitutes the Gaussian approximation

$$Z_q^{(g)}(u) = \frac{1}{\sqrt{u}} \left| \eta(iu) / \eta(i) \right|^{-2} , \quad (16)$$

where η is the Dedekind eta function

$$\eta(\tau) = q^{1/24} \prod_{n=1}^{\infty} (1 - q^n) , \quad q \equiv \exp(2\pi i\tau) . \quad (17)$$

This is a well known result in string theory and conformal field theory, and coincides³ with the partition function of a 2D conformal invariant free boson on a torus of modular parameter $\tau = iu$ [5, 6, 4].

Within this approximation, the interface partition function takes the form

$$Z = \lambda e^{-\sigma L_1 L_2} Z_q^{(g)}(u) . \quad (18)$$

For $u = 1$, i.e. $L_1 = L_2 \equiv L$, one recovers the well known finite size behaviour of the interface partition function given in Eq. (1),

$$Z = \lambda e^{-\sigma L^2} . \quad (19)$$

It has been already verified [4] that the inclusion of the one-loop contribution (18) allows to describe accurately finite size effects on asymmetric lattices ($u > 1$): these turn out to be strong enough to make the classical approximation (19) completely inadequate. However, this result does not give a definitive answer about the reliability of the CWM hypothesis expressed by Eq. (10): it is in fact well known that the Gaussian model is the fixed point of a wide class of possible effective descriptions [18]. To identify the particular effective Hamiltonian which describes the free fluid interface it is then crucial to test higher-order contributions.

Let us also stress that, among various possibilities, Eq. (10) is the simplest and most intuitive from a geometrical point of view. Moreover, it does not add any new free parameter and, even if this hypothesis is rather old [2], it has never been tested beyond the Gaussian approximation until recently [10].

³The constant $\eta(i)$ has been introduced just to normalize $Z_q^{(g)}(1) = 1$.

3 Two-Loop Calculation

In this section we calculate the contribution to the partition function Z from the term given in the Eq. (15) which is the first correction to the Gaussian Hamiltonian. We write Z in the form

$$\begin{aligned}
Z &= \lambda_o e^{-\sigma_o A} Z_q^{(g)}(u) Z_q^{(2l)}(u, \sigma_o A, \varrho_o) \quad (20) \\
Z_q^{(2l)} &= 1 + \frac{\varrho_o}{8\sigma_o A} \int [D\phi] \mathcal{H}_p[\phi] e^{-\mathcal{H}_g[\phi]} + O((\sigma A)^{-2}) \\
&= 1 + \frac{\varrho_o}{8\sigma_o A} \langle \int_0^1 d\xi_1 \int_0^1 d\xi_2 ((\nabla\phi)^2)^2 \rangle , \quad (21)
\end{aligned}$$

where the expectation value is taken in the free theory. In this section the subscript $_o$ is added to the bare quantities in order to distinguish them from the corresponding renormalized ones. In the Nambu-Goto model $\varrho_o = 1$.

Eq. (21) shows that the two-loop contribution can be expressed in terms of products of double derivatives of the free Green function. Wick's theorem gives

$$\begin{aligned}
\langle \int_0^1 d\xi_1 \int_0^1 d\xi_2 ((\nabla\phi)^2)^2 \rangle &= \left[3u^2 (\partial_{\xi_1}^2 G)^2 + 3u^{-2} (\partial_{\xi_2}^2 G)^2 + \right. \\
&\quad \left. 2\partial_{\xi_1}^2 G \partial_{\xi_2}^2 G + 4(\partial_{\xi_1} \partial_{\xi_2} G)^2 \right]_{\xi \rightarrow \xi'} \quad (22)
\end{aligned}$$

with

$$G(z - z') = \langle \phi(\xi) \phi(\xi') \rangle , \quad (23)$$

where we have introduced the complex variable $z = \xi_1 + iu\xi_2$.

Let us denote by $\{\omega\}$ the period lattice, namely the set of points of the complex plane of the form $\{\omega = m + inu, m, n \in Z\}$. Then the periodic boundary conditions can be written simply as

$$G(z + \omega) = G(z) . \quad (24)$$

The Green function should also satisfy

$$-\Delta \langle \phi(\xi) \phi(0) \rangle = \delta^{(2)}(\xi) - 1 \quad (25)$$

where

$$\Delta = u \frac{\partial^2}{\partial \xi_1^2} + \frac{1}{u} \frac{\partial^2}{\partial \xi_2^2} . \quad (26)$$

The -1 term on the right-hand side of Eq. (25) represents the subtraction of the zero mode due to the translational invariance of the interface in the z -direction: this is the standard procedure making Δ invertible in the subspace orthogonal to the zero mode (see for instance Ref. [22]).

The solution of the above equation can be expressed in terms of the Weierstrass σ function, defined through the infinite product

$$\sigma(z) = z \prod_{\omega \neq 0} \left(1 - \frac{z}{\omega}\right) e^{z/\omega + \frac{1}{2}(z/\omega)^2} . \quad (27)$$

We can write the solution as a sum of three terms

$$G(z) = -\frac{1}{2\pi} \ln|\sigma(z)| + \frac{\pi E_2(iu)}{12} \Re e(z^2) + \frac{1}{2u} (\Im m(z))^2 , \quad (28)$$

where $E_2(\tau)$ is the first Eisenstein series

$$E_2(\tau) = 1 - 24 \sum_{n=1}^{\infty} \frac{n q^n}{1 - q^n} , \quad q \equiv \exp(2\pi i\tau) . \quad (29)$$

The last term in Eq. (28) accounts for the zero mode subtraction, while the first two may be thought of as the real part of an analytic function $f(z)$, hence they satisfy $\Delta \Re e f(z) = 0$ outside the singularities at $z \in \{\omega\}$. For z near a node of the period lattice the second term is regular while the first one behaves like $-\frac{1}{2\pi} \ln|z - \omega|$ as it should in order to yield the correct normalization of the delta function. The coefficient of the second term is uniquely fixed by imposing the periodic boundary conditions of Eq. (24) (for a different, but equivalent form of the solution see for instance Ref. [22] p. 571).

The double derivative of the Green function can be easily calculated using the the formula

$$\wp(z) = -\frac{d^2}{dz^2} \ln(\sigma(z)) , \quad (30)$$

where $\wp(z)$ is the Weierstrass \wp -function. We need only the first few terms of its Laurent expansion about the origin

$$\wp(z) = \frac{1}{z^2} + \frac{\pi^4}{15} E_4(iu) z^2 + \dots , \quad (31)$$

where $E_4(\tau)$ is the second Eisenstein series. The double pole at the origin implies that the limit for $\xi \rightarrow \xi'$ in Eq. (22) is singular. In order to regularize

this theory we keep $\xi - \xi'$ different from zero by putting $z = e^{i\alpha}|z| = e^{i\alpha}\varepsilon/L_1$ where ε is used as an ultraviolet spatial cut-off. We get

$$Z_q^{(2l)} = 1 + \frac{\varrho_o}{\sigma_o} \left[\frac{A}{8\pi^2\varepsilon^4} + \frac{\cos(2\alpha)c(u)}{4\pi\varepsilon^2} + \frac{\cos(4\alpha)d(u)}{A} \right] + \frac{\varrho_o f(u)}{\sigma_o A} + O(\varepsilon) \quad , \quad (32)$$

with $c(u) = (\pi u E_2(iu)/3 - 1)$, $d(u) = \pi^2 u^2 E_4(iu)/60$ and

$$f(u) = \frac{1}{2} \left\{ \left[\frac{\pi}{6} u E_2(iu) \right]^2 - \frac{\pi}{6} u E_2(iu) + \frac{3}{4} \right\} \quad . \quad (33)$$

The three terms in the square brackets of Eq. (32) are cut-off dependent quantities. They can be reabsorbed in the renormalization of the couplings σ, λ and ϱ , respectively. In fact, putting $\sigma = \sigma_o + \delta\sigma_o$, $\lambda = \lambda_o + \delta\lambda_o$ and $\varrho = \varrho_o + \delta\varrho_o$ in Eq. (20), comparison with Eq. (32) yields

$$\delta\sigma_o = -\frac{\varrho_o}{8\pi^2\varepsilon^4\sigma_o} \quad (34)$$

$$\delta\lambda_o = \frac{\lambda_o\varrho_o \cos(2\alpha)c(u)}{4\pi\varepsilon^2\sigma_o} \quad (35)$$

$$\delta\varrho_o = \varrho_o \cos(4\alpha) \frac{d(u)}{f(u)} \quad . \quad (36)$$

Of course the renormalized quantities σ, λ and ϱ should not depend on the regularization scheme and in particular on the choice of the parameter α . On the other hand, choosing $\alpha = \frac{\pi}{8}$, we get $\delta\varrho_o = 0$, which shows that ϱ is not renormalized, at least at the first perturbative order. Thus we can safely put the Nambu-Goto value $\varrho = 1$ in the final formula

$$Z = \frac{\lambda}{\sqrt{u}} e^{-\sigma L_1 L_2} \left| \eta(iu) / \eta(i) \right|^{-2} \left[1 + \frac{f(u)}{\sigma L_1 L_2} + O\left(\frac{1}{(\sigma L_1 L_2)^2} \right) \right] \quad , \quad (37)$$

where $f(u)$ is defined in Eq. (33). Note that Eq. (37) is symmetric under the exchange $L_1 \leftrightarrow L_2$ as a consequence of the functional relation

$$E_2\left(-\frac{1}{\tau}\right) = \tau^2 E_2(\tau) - i \frac{6\tau}{\pi} \quad . \quad (38)$$

Similarly, it can be shown that also Eqs. (34-36) are symmetric under such exchange. Our two-loop result coincides with the one obtained some years ago in the context of string theory [11], using the ζ -function regularization.

The fact that two completely independent regularization schemes tell us that the coupling ϱ is not renormalized suggests that this a general property, even if we have not yet found a rigorous argument to support it. Note that in our derivation the splitting between the cut-off dependent part and the remainder in Eq. (32) is a crucial point. Such a separation arises in a natural way in our regularization, but it is conceivable that different cut-off schemes might generate a different splitting. We notice, however, that the functional form of the two-loop contribution is preserved by the modular invariance. This is not obvious in our derivation because, for sake of simplicity, we dealt with a rectangular torus with a purely imaginary modulus $\tau = iu$. It is possible to develop the theory on a generic torus associated to an arbitrary complex modulus τ . Any physical quantity must be invariant under the two generators of modular group:

$$S : \tau \rightarrow -1/\tau \quad (39)$$

$$T : \tau \rightarrow \tau + 1. \quad (40)$$

The terms in the square brackets of Eq. (32) are not modular invariant because the angle α has not an intrinsic geometric meaning. On the contrary, the function $F(iu) = f(u)$ which yields the functional form of the two-loop contribution (37) is modular invariant. Its form in a general frame (i.e. τ arbitrary complex number) is given by

$$F(\tau) = \frac{1}{2} \left\{ \left| \frac{\pi}{6} \Im m(\tau) E_2(\tau) - \frac{1}{2} \right|^2 + \frac{1}{2} \right\} . \quad (41)$$

Notice that Eq. (37) has no longer the functional form of the classical approximation (19) even on symmetric lattices: for $u = 1$ it can be easily seen that Eq. (37) gives

$$Z = \lambda e^{-\sigma L^2} \left(1 + \frac{1}{4\sigma L^2} \right) , \quad (42)$$

where the identity $E_2(i) = \frac{3}{\pi}$ has been used, which follows directly from Eq. (38).

Let us stress finally that no new free parameter is introduced within this approach.

4 Observables and Monte Carlo Simulations

Let us discuss the observables of the Ising model that we can use to test the functional form of the interface free energy.

In the finite geometry the degeneracy of the ground state is removed: the energy of the symmetric, Z_2 invariant, ground state is separated by a small energy gap ΔE (or inverse tunneling correlation length) from the antisymmetric ground state energy.

This energy splitting is due to tunneling between the two vacua and is directly linked to the free energy of the interface. In the dilute gas approximation, in which multi-interface configurations are summed over, but interactions between interfaces are neglected, the energy splitting is directly proportional to the interface partition function Z , where Z is given by Eqs. (18,19,37). It is then easy to show (see e.g. [23]) that

$$\Delta E = Z(\sigma, L_1, L_2) \quad , \quad (43)$$

where the usual factor 2 has been reabsorbed into the parameter λ appearing in the definitions of Z . Let us notice that λ has the physical dimensions of an energy. In the scaling region of the Ising model all dimensional quantities should depend on β according to the scaling law

$$\xi(\beta) \simeq \xi_\infty \left(1 - \frac{\beta_c}{\beta}\right)^{-\nu} \quad , \quad (44)$$

where ξ_∞ is the bulk correlation length in the continuum limit. The most precise estimates for ν are in the range from 0.624 to 0.630 [13, 25]. Since the interface tension is the only dimensional physical quantity appearing in the interface free energy, in the following we express all physical observables in units of the square root of the interface tension $\sqrt{\sigma_\infty}$ according to the scaling law

$$\sqrt{\sigma(\beta)} = \sqrt{\sigma_\infty} \left(1 - \frac{\beta_c}{\beta}\right)^\nu \quad . \quad (45)$$

The measurements of the energy gap ΔE , for different choices of the lattice sizes, provides then a first direct check on the functional form of the interface free energy and allows one to estimate the interface tension σ . To this end, we have used two different methods, as explained in the following two sections.

A second observable we have used to check our theoretical prediction is the surface energy E_S defined by

$$E_S(\sigma, L_1, L_2) = -\frac{1}{Z} \frac{\partial Z}{\partial \beta} \quad . \quad (46)$$

This observable is particularly useful because it enables us to isolate explicitly quantum contributions beyond the Gaussian one, as it will be discussed below.

Before describing the method we used to estimate these quantities, let us make some general remarks, independent from the observable and MC method used, on the range of values of β and on the lattice sizes where our formulae can be used.

Applying Eq. (37), one should pay attention to avoid spurious effects like the incomplete restoration of rotational invariance and the residual presence of lattice artifacts, as already discussed. To this end we made our simulation in the scaling region of the Ising model: the lowest temperature used corresponds to $\beta = 0.240$. (In Tab. 1 we present besides other quantities to be introduced below estimates for the bulk correlation length of the Ising model at the β -values used in the present study. The MC estimate is taken from Ref. [15]. The other estimates are based on the low temperature series that was extended to 15th order by Arisue [16]. We analysed the series with the help of inhomogeneous differential approximants [17]. The numbers in the table are the results from the [1; 7, 7] approximation.)

The expansion parameter σA should be small enough to justify the perturbative calculation.

Interactions between interfaces should be negligible, which means that the dilute gas approximation must be satisfied: the dominant contribution in the probability of creating an interface is proportional to $e^{-\sigma A}$. Too small lattice size can give rise to a high density of interfaces and to non-negligible interactions.

Finally, the smallest size of the lattice (L_1 in our conventions) should not only be greater than the bulk correlation length but also greater than the (inverse) deconfinement temperature of the dual gauge model. In fact, by duality (see for instance [24], see also [4]), the broken phase of the Ising model on an asymmetric 3D lattice corresponds to the confined phase of the 3D Z_2 gauge model at a finite temperature $T^{(g)} = 1/L_1$.

Precise information on the finite temperature deconfinement transition can be found, for instance, in [26]. β is mapped to the gauge coupling constant $\tilde{\beta} = -\frac{1}{2} \ln \tanh \beta$. For each β there exists a value $L_c(\beta)$ such that for $L_1 \leq L_c$ the gauge system is in the deconfined phase, and Eq. (37) cannot be applied.

The values of L_c for the β 's used are given in Tab. 1. These have been

obtained using data taken from Ref. [26] and the scaling law

$$\frac{1}{L_c(\beta)} = T_c^{(g)} (\tilde{\beta}_c - \tilde{\beta}(L_c))^\nu , \quad (47)$$

where $T_{(g)}^c = 2.3(1)$, $\tilde{\beta}_c \simeq 0.7614$ and $\nu \simeq 0.630$ (see [12]).

4.1 Energy Gap: the Time-Slice Correlations Method

The first method we have used to extract the energy splitting ΔE follows the procedure explained in Ref. [27] (see also Refs. [28, 4]); we refer to it as the *time-slice correlations* method (TSC).

Consider a cylindrical geometry, with $t \gg L_1, L_2$ and periodic boundary conditions in all directions, and define the time-slice magnetization S_k , where $k = 0, 1, \dots, t/2$, as

$$S_k \equiv \frac{1}{L_1 L_2} \sum_{n_1=1}^{L_1} \sum_{n_2=1}^{L_2} s_{\vec{n}} , \quad (48)$$

with $\vec{n} \equiv (n_1, n_2, k)$. If one computes the two-point correlation function

$$G(k) \equiv \langle S_0 S_k \rangle , \quad (49)$$

the low energy levels of the transfer matrix spectrum can be obtained from the asymptotic k -dependence of $G(k)$

$$G(k) \cdot Z_I = c_0^2 \left(e^{-k\Delta E} + e^{-(t-k)\Delta E} \right) + c_1^2 \left(e^{-k\Delta E'} + e^{-(t-k)\Delta E'} \right) + \dots \quad (50)$$

$$Z_I = 1 + e^{-t\Delta E} + \dots \quad (51)$$

where $Z_I \equiv \text{tr } e^{-tH}$ is the partition function of the Ising model in the transfer matrix formalism.

$\Delta E'$ is the energy of the first (antisymmetric) excited state and turns out to be (at least) one order of magnitude greater than ΔE in the range of parameters we have used. The coefficient c_0 corresponds to the magnetization expectation value and can be used to check the consistency of the MC results.

To perform our MC simulations we used a Swendsen-Wang cluster algorithm [30]. For each value of β considered, i.e. $\beta = 0.2246, 0.2258$ and

0.2275, L_1 and L_2 ranged from 10 to 35. We usually fixed $t = 120$, using, for simulations with particularly large L_1 and L_2 , bigger sizes $t = 240 - 360$. The values of the energy gap ΔE , extracted using Eq. (50), are reported in Tabs. 2, 3 and 4 (for Tab. 4 see also the table caption)⁴; the confidence levels of these fits are always above 70%.

Using this approach one should pay attention to correlations in MC time. In particular it turns out that the two-point correlation functions $G(k)$ are affected by very strong cross-correlations in MC time. To take under control this problem, we followed the procedure used in Ref. [4], scattering the evaluation of time-slice correlations in Monte Carlo time. This has the advantage of reducing the cross-correlation matrix to an almost-diagonal form and simplify the non-linear fitting procedure. For each β and each lattice we made about $0.6 - 1.2 \cdot 10^6$ sweeps (after thermalization) with $1 - 2 \cdot 10^3$ measurements/observable. A standard jackknife procedure was used to evaluate errors.

Fig. 1 shows a histogram of the magnetization for a typical lattice size. Almost all configurations contain zero or two interfaces, which indicates that the dilute gas approximation is respected. The plateau corresponds to configurations of the system with two interfaces (because of the periodic boundary conditions in the z -direction). It is easy to see that the presence of more interfaces would have the effect of strongly modify it. The two peaks correspond to configurations without interfaces.

4.2 Energy Gap: the Boundary Flip Method

Another method (which we refer to as the *boundary flip* (BF) method) to evaluate the energy gap ΔE was introduced by one of the authors in Refs. [31, 32].

We consider a system which allows both periodic (p) and antiperiodic (a) boundary conditions (bc). The partition function of this system is given by

$$Z = Z_a + Z_p = \sum_{bc} \sum_{\{s_i=\pm 1\}} e^{-\beta H(s,bc)} \quad (52)$$

and the fraction of configurations with antiperiodic boundary conditions is given by

$$\frac{Z_a}{Z} = \frac{1}{Z} \sum_{\{s_i=\pm 1\}} e^{-\beta H(s,a)} = \frac{1}{Z} \sum_{bc} \sum_{\{s_i=\pm 1\}} \delta_{bc,a} e^{-\beta H(s,bc)} = \langle \delta_{bc,a} \rangle . \quad (53)$$

⁴Some of these data have appeared preliminarily in Ref. [29].

An analogous result can be found for periodic boundary conditions.

We can express the ratio Z_a/Z_p as a ratio of observables in this system,

$$\frac{Z_a}{Z_p} = \frac{\langle \delta_{bc,a} \rangle}{\langle \delta_{bc,p} \rangle} \quad (54)$$

which turns out to be directly connected to the energy gap ΔE .

To see this, let us express the partition functions of the periodic and antiperiodic Ising system in terms of the transfer matrix \mathbf{T} . The antiperiodic boundary conditions are represented by a spin-flip operator \mathbf{P} , which flips the sign of all spins in a given z -slice.

The partition function of the periodic system is given by

$$Z_p = \text{Tr} \mathbf{T}^t \quad , \quad (55)$$

while the partition function of the antiperiodic system is given by

$$Z_a = \text{Tr} \mathbf{T}^t \mathbf{P} \quad . \quad (56)$$

Since the operators \mathbf{T} and \mathbf{P} commute, they have a common set of eigenfunctions. Say the eigenvalues of \mathbf{T} are λ_i and those of \mathbf{P} are p_i . The possible values of p_i are 1 and -1 . States that are symmetric in the magnetization have $p_i = 1$ and those that are antisymmetric have $p_i = -1$. The partition functions take the form

$$Z_p = \sum_i \lambda_i^t \quad (57)$$

and

$$Z_a = \sum_i \lambda_i^t p_i \quad . \quad (58)$$

Let us consider the ratio of the partition functions in the low temperature phase. If we assume that

$$\lambda_{0s}, \lambda_{0a} \gg \lambda_{1s}, \lambda_{1a}, \dots \quad (59)$$

then, ignoring terms of order $O[(\lambda_{1s}/\lambda_{0s})^t]$, it is easy to show that

$$\left(\frac{\lambda_{0a}}{\lambda_{0s}} \right)^t = \frac{Z_p - Z_a}{Z_p + Z_a} = 1 - 2 \langle \delta_{bc,a} \rangle \quad . \quad (60)$$

The interface free energy (inverse of the tunneling mass) is then given by

$$\Delta E = -\ln(\lambda_{0a}/\lambda_{0s}) = -\frac{1}{t} \ln(1 - 2 \langle \delta_{bc,a} \rangle) \quad . \quad (61)$$

Assuming that the number of interfaces is even for periodic boundary conditions and odd for anti-periodic boundary conditions, the dilute gas approximation leads to exactly the same relation between the interface free energy and the boundary statistics [31].

We have used the BF method at $\beta = 0.2240$ for a large number of lattices, as reported in Tab. 5. In a few cases we studied two or three values of t , in order to check the stability of the results. In general, however, the t value needed is smaller than the one we would have needed when using the TSC method. For this reason, the BF method is particularly useful near the critical point where large L_1 and L_2 must be used.

For the determination of the ratio of partition functions Z_a/Z_p we employed the boundary cluster algorithm proposed by one of the authors [31, 32].

For each simulation given in Tab. 4 (case *c*) and in Tab. 5 we have made, after thermalization, $0.7 - 1.4 \cdot 10^5$ sweeps, depending on the lattice size.

Moreover, the BF method bypasses the fitting procedure of Eq. (50) required by the TSC method, reducing from $t/2$ to one ($< \delta_{bc,a} >$) the observables needed to evaluate E . This allows to save MC time as well as drastically reduces the problems connected to correlations in MC time.

4.3 Surface Energy

As stated above, one can also measure the surface energy and compare the MC results with the CWM predictions.

If one assumes Eq. (37), it follows from Eq. (46) ($\sigma' \equiv \partial_\beta \sigma$ and $\lambda' \equiv \partial_\beta \lambda$) that

$$E_S^{(CWM)}(\sigma, L_1, L_2) = \sigma' L_1 L_2 - \frac{\lambda'}{\lambda} - \frac{1}{Z_q^{(2l)}} \partial_\beta Z_q^{(2l)} . \quad (62)$$

On the other hand, if one uses Eq. (19) or Eq. (18) one gets

$$E_S^{(1l)}(\sigma, L_1, L_2) = \sigma' L_1 L_2 - \frac{\lambda'}{\lambda} , \quad (63)$$

because one-loop quantum contributions do not depend on β . In particular, from Eq. (37) one expects corrections proportional to $(Area)^{-1}$ due to the two-loop corrections to the CWM which would be absent for a pure Gaussian model.

To measure the surface energy we follow the MC procedure which was already used in Ref. [33]. Consider again the ratio Z_a/Z_p . From Eq. (60)

one can express the ratio Z_a/Z_p in terms of the two largest transfer matrix eigenvalues

$$\frac{Z_a}{Z_p} \simeq \frac{t}{2} \left(1 - \frac{\lambda_{0a}}{\lambda_{0s}} \right), \quad (64)$$

where we again ignore terms of order $O\left[(\lambda_{1s}/\lambda_{0s})^t\right]$. In addition we assume that $t \ll 1/\Delta E$. This means that for periodic boundary conditions the configurations without an interface dominate while for anti-periodic boundary conditions there is only one interface present in almost all configurations. Then, within this approximation, one obtains from Eq. (64) a definition of surface energy which does not depend on the extension t , and

$$E_S \equiv E_p - E_a, \quad (65)$$

with $E_p = \langle H \rangle_p$ and $E_a = \langle H \rangle_a$.

We have applied this method at $\beta = 0.240$ for many lattice sizes with t ranging from 10 to 40. The surface energies E_S for each lattice are given in Tab. 6.

4.4 Local Demon Algorithm

The variance of the energy stems to a major part from fluctuations on small scales. Hence an optimally implemented local algorithm is superior to a cluster algorithm in solving this particular problem. We used a micro-canonical demon algorithm [35, 36, 37] in combination with a particularly efficient canonical update [38] of the demons. This type of algorithm circumvents the frequent use of random numbers. The algorithm is implemented using the multi-spin coding technique [36, 37]. Every bit of a computer word carries one Ising spin. In order to avoid restrictions of the geometry we simulate 32 (the number of bits in a word) independent systems.

We have chosen demons that carry the energies 4, 8, and 16. We take one demon for each lattice site.

First we used the cycle described in [33] to simulate the systems with periodic and anti-periodic boundary conditions independently. However, it turned out that in contrast to the situation close to the roughening transition, near the bulk critical point also frequent updates of the demons carrying the energies 8 and 16 are needed to obtain autocorrelation times close to that of the Metropolis algorithm. As one can see from the CPU times summarized in Tab. 1 of Ref. [33], this would mean a considerable increase of the CPU time needed.

We could, however, overcome this problem by simulating systems with periodic and anti-periodic boundary conditions in a single simulation and coupling them to the same demon system. It turned out that for our particular choice of the update cycle, the integrated autocorrelation time of $E_p - E_a$ was almost one order of magnitude smaller than the integrated autocorrelation time of E_p and E_a as separate quantities.

The cycle that we used mostly can be explained as follows. The simulation was done by performing a cycle of 6 groups, where each group consisted of a *micro-canonical* update of the 32 periodic systems and the demon, the 32 anti-periodic systems plus the demon and a *translation* or a shift with respect to the 32 copies of the spin system of the demon layer with energy 4, 8, or 16 (alternating). Each group was finished by updating the demons with energy 4. The whole cycle was completed by updating the demons with energy 8. We performed a measurement twice in this cycle.

For the $24 \times 24 \times 40$ lattice at $\beta = 0.24$ we observed the integrated autocorrelation times $\tau_p = 5.3$ and $\tau_a = 5.1$ of the energy with periodic and anti-periodic boundary conditions, while the integrated autocorrelation time of the surface energy $\tau_s = 0.6$ was about one order of magnitude smaller. As unit of the autocorrelation time we took one cycle. The simulation with 200000 cycles took about 104 h on a SPARC 10 workstation.

We used the drand48 random number generator from the C-library and the G05CAF from the NAGLIB. For some choices of the parameters we simulated with both random number generators. The results are consistent within the error bars.

5 Monte Carlo Data Analysis

In this section we compare the CWM predictions with data extracted from MC simulations for the two observables defined in Eqs. (43,46).

5.1 FSEs of the Interface Free Energy

Let us first discuss the fits of the energy gap formula Eq. (43) to the data given in Tabs. 2–5, using different functional forms for the interface partition function Z , in analogy with Refs. [10, 29].

We call *classical*, *one-loop* and *two-loop* fits those made with Z given by Eq. (19), Eq. (18) and Eq. (37), respectively.

The values of the energy gaps we used range over nearly four orders of magnitude, the biggest value being $\Delta E = 0.0444$ at $\beta = 0.2246$, for a

$L_1 = L_2 = 13$ lattice size, and the smallest $\Delta E = 0.09 \cdot 10^{-4}$ at $\beta = 0.2275$, with $L_1 = L_2 = 26$ (see Tabs. 2 and 4).

To obtain estimates of ΔE for large lattice sizes the BF method is more efficient than the TSC method. For this reason we have principally used it at $\beta = 0.2240$ (Tab. 5), which (from our set of values) is the closest to to the critical point. Rather large lattices are needed here (see also Tab. 1). The BF algorithm has been also used to take some measurements at $\beta = 0.2275$, to obtain energy gaps for particularly small value of the two-loop contribution parameter

$$x \equiv f(u)/(\sigma A) \quad , \quad (66)$$

where $f(u)$ is defined by Eq. (33), with $u = L_2/L_1$ and $A = L_1 L_2$.

In Tab. 7 we report the fits we made for each β : the reduced χ^2 of the classical fits turns out to be always more than one order of magnitude greater than those of one and two-loop fits, in agreement with what was already shown in [4, 10]. Moreover, two-loop fits show a level of confidence which is higher than the one-loop fits for all β 's: this is the first evidence that the two-loop corrections discussed above correctly describe the data.

For $\beta = 0.2246, 0.2258$ and 0.2275 the MC data⁵ are given in Fig. 2, while those referring to $\beta = 0.2240$, which range over a rather different scale both in ΔE and in A , are plotted in Fig. 3. The lines represent the best two-loop fits; their values in correspondence of the MC data are also given in Tabs. 2–5 ($\Delta E^{(CWM)}$).

Both the high χ^2 values of the fits and the clear u -dependence of the MC data in Fig. 2 and Fig. 3 show that the classical contribution, Eq. (19), being only function of A and not of u is completely ruled out.

Therefore, from now on, we concentrate on the one and two-loop functional forms.

Let us now make some further considerations on the different results one obtains with the one-loop and the two-loop approximations to the CWM. The parameter x , at fixed β and for any given lattice, gives the relative weight of the two-loop correction with respect to the classical and one-loop contributions (see Eq. (37)). One expects that a fit on a sample of data for which $x \ll 1$ should give consistent results both at one and two-loop and that, as one increases the value of x , the fits made with the two-loop contributions should have better confidence levels than those made with the

⁵Some data at $\beta = 0.2275$ and $\beta = 0.2240$ do not appear in the figures: their behaviour is analogous to that of the other data. They have been omitted only in order to have a better resolution in the figures.

one-loop only. Finally, if the CWM is the correct picture, an upper value of x should exist at which higher order corrections should become important and fits with the two-loop contribution should start to show higher χ^2 's.

The values of x for all samples of data are given, in Tabs. 2–5 in the last columns, while the values of σ which have been used to evaluate it (see Eq. (66)) are given in Tab. 7 (the differences between the one and two-loop values are not appreciable in this case). One can see that x ranges from 0.03 up to the rather large value of 0.27.

In order to make more stringent fits, we can use all the data we have by expressing σ through the scaling law (45): the free parameters then become $\lambda/\sqrt{\sigma}$, σ_∞ and ν . With this assumption Eqs. (18,37) take the form

$$Z_{1l} = \frac{\lambda}{\sqrt{\sigma}} \sqrt{\sigma_\infty} (1 - \beta_c/\beta)^\nu e^{-\sigma_\infty A(1-\beta_c/\beta)^{2\nu}} Z_q^{(g)}(u) \quad (67)$$

$$Z_{2l} = Z_{1l} \cdot \left[1 + \frac{f(u)(1 - \beta_c/\beta)^{-2\nu}}{\sigma_\infty A} + O\left(\frac{(1 - \beta_c/\beta)^{-4\nu}}{(\sigma_\infty A)^2}\right) \right] \quad (68)$$

According to the usual attitude, we make the fits also using the other scaling law

$$\sqrt{\sigma(\beta)} = \sqrt{\sigma_\infty} \left(\frac{\beta}{\beta_c} - 1 \right)^\nu \quad (69)$$

with the obvious modifications of Eqs. (67,68).

We performed the fits on the samples of energy gaps

$$\{ \Delta E(x) \mid x \leq x_{cut} \} \quad , \quad (70)$$

starting from the first six data ($x_{cut} = 0.058$) and adding two data each time, so that the last fits contain all the 56 data. The corresponding χ^2/dof obtained with the one-loop (empty circles) and two-loop (full circles) formulae written above, as functions of x_{cut} , are reported in Fig. 4.

From the figure one can see that the one-loop formula (67) has a 50% confidence level (or more) for $x_{cut} \sim 0.15$, which corresponds to 36 data over 56 of our sample, while the two-loop formula (68) reaches, with the same confidence level, $x_{cut} \sim 0.20$, which corresponds to 47 data. The fact that both fits on the first sample have a reduced χ^2 greater than one is instead due to the lack of statistics (only 6 data points). For $x_{cut} > 0.2$, the reduced χ^2 of the fits made with the two-loop correction indicates that higher order corrections could be important. Notice, however, that the confidence levels for the two-loop fits are better than those for the one-loop fits. The parameter of the fits turns out to be very stable, for both types of fits,

until the $\chi^2/dof \approx 1$: these are given in Tab. 8 for the two limiting samples discussed above. The results obtained for σ_∞ and ν are consistent with the values reported in the literature and, almost, with each other, the only difference being in the constant $\lambda/\sqrt{\sigma}$. Let us point out that, if the two-loop contributions obtained from the CWM Hamiltonian (11) are physical, one expects the two formulae (67,68) to give the same constant when the above fitting procedure is applied to a sample with $x_{cut} \approx 0$. As we can observe looking at our sample of data, it is rather difficult to reduce x_{cut} below 0.05 without spoiling the reliability of the statistics of our analysis, but we can significantly check the constance of $\lambda/\sqrt{\sigma}$ making fits on (independent) samples in which the x values included are approximately constant. That is, we define the sample

$$\{ \Delta E(x) \mid x_i \leq x \leq x_{i+\epsilon} \} \quad (71)$$

and we denote with x_{av} the average value of x within each sample.

The results are given in Tab. 9 and in Fig. 5. It turns out that both the ν and σ_∞ values are very stable on the whole sample, discarding the last one where x_{av} is too big. However, while the one-loop and two-loop constants are compatible for $x_{av} = 0.04 - 0.07$, moving toward greater x_{av} values $\lambda/\sqrt{\sigma}$ increases systematically in the one-loop case while remains stable when the two-loop formula is used. This indicates that the absence of the $1/(\sigma A)$ corrections in the Gaussian formula is artificially compensated by the enhancements of its constant, already for $x_{av} \sim 0.1$. As a final comment, let us note that a comparison with a semiclassical ϕ^4 approach [8] suggests to fix $\lambda/\sqrt{\sigma}$ to $[4 \Gamma(3/4)/\Gamma(1/4)] \simeq 1.352$, in good agreement with the two-loop value $\simeq 1.33(1)$ of Tab. 8 and Tab. 9.

5.2 FSEs of the Surface Energy

In this section we discuss the finite size behaviour of the interface partition function from MC measurements of the surface energy defined by Eq. (46).

As already said in Sec. 4.4, this approach has the advantage that the two-loop contribution appears as an additive correction to the surface free energy calculated at the Gaussian (and classical) level, as given by Eq. (62) and Eq. (63), respectively. We decided to make our simulations at $\beta = 0.240$ also because very precise estimates of σ and σ' (two of the three parameters on which Eqs. (62,63) depends on) are known,

$$\sigma = 0.0590(2) \quad , \quad \text{from [3]} \quad (72)$$

$$\sigma' = 3.813(2) \quad , \quad \text{from [39]} \quad . \quad (73)$$

Our preliminary step is to assume as external inputs these values and, assuming they are not biased, to use them to test the reliability of the functional form of the second order quantum contribution to the interface free energy.

Let us define the following surface energy differences (at fixed β)

$$\Delta E_S(L) = E_S(2L, L/2) - E_S(L, L) \quad (74)$$

considering two different lattices, one with $u = L_2/L_1 = 4$ and the other with $u = 1$, but with the same area $A = L_1 L_2 = L^2$. Then, from Eqs. (63,62) one obtains

$$\Delta E_S^{(1l)}(L) = 0 \quad (75)$$

$$\Delta E_S^{(CWM)}(L) = \frac{\partial_\beta Z_q^{(2l)}}{Z_q^{(2l)}} \Big|_{u=4} - \frac{\partial_\beta Z_q^{(2l)}}{Z_q^{(2l)}} \Big|_{u=1} . \quad (76)$$

The theoretical prediction of the Gaussian model requires these differences to be zero, while that of the CWM at two-loop does not depend any more on the third parameter, λ'/λ . Eq. (76) can be written explicitly as

$$\Delta E_S^{(CWM)} = \frac{\sigma'}{\sigma^2 L^2} [f(4) - f(1)] \quad (77)$$

where $f(u)$ is given by Eq. (33) and in the two points we are considering takes the values $f(1) = 0.25$ and $f(4) \simeq 1.52$.

Using the MC data given in Tab. 6 (taken at $\beta = 0.240$) one can easily construct these differences. They are given in the first column of Tab. 10, where we have assumed $L \equiv 2L_1 = L_2/2$. It is clear that all these data are not compatible with zero. Assuming the validity of Eqs. (72,73) and plugging the values into Eq. (77) we obtain the theoretical predictions reported in the second column of Tab. 10. Monte Carlo data and theoretical predictions are plotted in Fig. 6

A nice $Area^{-1}$ behaviour is clearly seen in the MC data for $L \geq 16$, in good agreement with Eq. (77). Comparing the last column of Tab. 6 with Tab. 10 one sees that this corresponds to $x \sim 0.1$, while for $x \geq 0.13$ higher order corrections would be needed and for $x \geq 0.20$ the two-loop contributions are definitively too small.

Then we follow the same approach of the preceding section, that is we assume different forms of the free energy and choose among them using the reduced χ^2 s of the fits with equal number of parameters. In this case, our main parameters are fixed from the fits.

We fit Eq. (62), which can be written explicitly as

$$E_S^{(CWM)}(L_1, L_2) = \sigma' L_1 L_2 + \frac{\sigma'}{\sigma^2 L_1 L_2} f(u) - \frac{\lambda'}{\lambda} \quad (78)$$

and Eq. (63). The results are given in Tab. 11, where the parameters refer to the two-loop fits while, for the Gaussian fits, only the reduced χ^2 's are given in the second column.

Finally, we can make an interesting check comparing the ratio of σ' and σ with the equation one obtains from the asymptotic scaling laws. Taking the derivative with respect to β in Eq. (69), one gets

$$\frac{\sigma'}{2\sigma} = \frac{\nu}{(\beta - \beta_c)} \quad (79)$$

In order to compute this ratio we take the last two results of Tab. 11, the values of Eqs. (72,73) and assume $\nu \simeq 0.63$. The results are given in the fourth column of Tab. 12. Notice that the RHS of Eq. (79) should also be obtained from λ'/λ : from Tab. 11 one sees that the two estimates agree within errors.

On the other side, one can also assume this ratio as an input to evaluate the critical index ν , inverting Eq. (79); one gets

$$\nu = \frac{\sigma'(\beta - \beta_c)}{2\sigma} \quad (80)$$

The corresponding values are given in the last column of Tab. 12. The agreement with the expected values is good, though the errors are still large.

6 Conclusions

In this paper we have demonstrated that the finite size effects of interface properties in the 3D Ising model are rather well described by the two-loop expansion of the CWM. Our MC data for the energy gap and the surface energy prove that there are corrections to the Gaussian approximation, and the various fits indicate that these corrections are indeed given (up to even higher corrections) by the two-loop result, with no extra coefficients introduced into the the game. Since there is (yet) no rigorous proof that the two-loop corrections are universal (i.e., independent from the regularization scheme) we have to consider the predictive power of the two-loop CWM model a little bit as a miracle. We consider the present contribution as a first step towards a deeper understanding of the physics of rough interfaces in terms of effective models.

References

- [1] M. P. Gelfand and M. E. Fisher, *Physica* **A 166** (1990) 1
V. Privman, *Int. J. Mod. Phys.* **C 3** (1992) 857
- [2] F. P. Buff, R. A. Lovett and F. H. Stillinger Jr., *Phys. Rev. Lett.* **15**
(1965) 621
- [3] M. Hasenbusch and K. Pinn, *Physica* **A 192** (1993) 342
- [4] M. Caselle, F. Gliozzi and S. Vinti, *Phys. Lett.* **B 302** (1993) 74
- [5] C. Itzykson and J. B. Zuber, *Nucl. Phys.* **B 275**[FS17] (1986) 580
- [6] B. Bunk, *Int. J. Mod. Phys.* **C 3** (1992) 889
- [7] M. E. Fisher, *J. Phys. Soc. Japan Suppl.* **26** (1969) 87
M. E. Fisher and V. Privman, *J. Stat. Phys.* **33** (1983) 385
E. Brézin and J. Zinn-Justin, *Nucl. Phys.* **B 257**[FS14] (1985) 867
- [8] G. Münster, *Nucl. Phys.* **B 340** (1990) 559
- [9] R. K. P. Zia, *Nucl. Phys.* **B 251** [FS13] (1985) 676
- [10] P. Provero and S. Vinti, preprint DFTT 58/93, TPI-MINN 93/46-T,
hep-lat 9310028
- [11] K. Dietz and T. Filk, *Phys. Rev.* **D 27** (1983) 2944
- [12] M. Caselle, R. Fiore, F. Gliozzi, P. Guaita and S. Vinti, preprint DFTT
57/93, to appear in *Nucl. Phys.* **B**
M. Caselle, F. Gliozzi and S. Vinti, *Nucl. Phys.* **B** (Proc. Suppl.) **34**
(1994) 263
For a review on the subject see F. Gliozzi, *Acta Phys. Pol.* **23 B** (1992)
971
- [13] C. F. Baillie, R. Gupta, K. A. Hawick and G. S. Pawley, *Phys. Rev.*
B 45 (1992) 10438
- [14] M. Hasenbusch, PhD-thesis, Universität Kaiserslautern (1992)
- [15] M. Hasenbusch, K. Rummukainen and K. Pinn, in preparation

- [16] H. Arisue, *Phys. Lett.* **B 322** (1994) 224
- [17] M.E. Fisher and H. Au-Yang, *J. Phys. A* **12** (1979) 1677
- [18] M. Lüscher, *Nucl. Phys.* **B 180** (1981) 317
- [19] P. Olesen, *Phys. Lett.* **B 160** (1985) 144
- [20] V. S. Dotsenko, G. Harris, E. Marinari, E. Martinec, M. Picco and P. Windey, *Phys. Rev. Lett.* **71** (1993) 811
- [21] M. Caselle, F. Gliozzi and S. Vinti, *Nucl. Phys.* **B** (Proc. Suppl.) **34** (1994) 726
- [22] C. Itzykson and J-M. Drouffe, *Statistical field theory*, Cambridge (1989)
- [23] S. Coleman, *Aspects of symmetry*, Cambridge (1985)
- [24] J.M. Drouffe and J.B. Zuber, *Phys. Rep.* **C 102** (1983) 1
- [25] J.-C. Le Guillou and J. Zinn-Justin, *Phys. Rev.* **B 21** (1980) 3976
- [26] S. Wansleben and J. Zittarz, *Nucl. Phys.* **B 280** (1987) 108
- [27] S. Klessinger and G. Münster, *Nucl. Phys.* **B 386** (1992) 701
- [28] K. Jansen, J. Jersak, I. Montvay, G. Münster, T. Trappenberg and U. Wolff, *Phys. Lett.* **B 213** (1988) 203
- [29] M. Caselle, F. Gliozzi, P. Provero and S. Vinti, *Nucl. Phys.* **B** (Proc. Suppl.) **34** (1994) 720
- [30] R.H. Swendsen and J.-Sh. Wang, *Phys. Rev. Lett.* **58** 86 (1987)
- [31] M. Hasenbusch, *J. Phys.* (Paris) **I 3** 753 (1993)
- [32] M. Hasenbusch, *Physica* **A 197** 423 (1993)
- [33] M. Hasenbusch and K. Pinn, *Physica* **A 203** 189 (1994)
- [34] U. Wolff, *Phys. Rev. Lett.* **62** 361 (1989); *Nucl. Phys.* **B 322** 759 (1989)
- [35] M. Creutz, *Phys. Rev. Lett.* **50** (1983) 1411

- [36] M. Creutz, G. Bhanot and H. Neuberger, *Nucl. Phys.* **B 235** [FS11] (1984) 417
- [37] M. Creutz, K.J.M. Moriarty and M. O'Brien, *Comput. Phys. Comm.* **42** (1986) 191
- [38] K. Rummukainen, *Nucl. Phys.* **B 390** (1993) 621
- [39] N. Ito, *Physica* **A 196** (1993) 591

β	L_c	$L_1^{(min)}$	$\zeta_{\text{bulk}}^{\text{MC}}$	$\zeta_{\text{bulk}}^{\text{IDA}}$
0.2240	12.1	18		4.527
0.2246	10.5	13		3.926
0.2258	8.5	12		3.170
0.2275	6.8	10	2.62(2)	2.556
0.2400	3.4	8		1.251

Tab. 1. The first column shows the β -values used in the present study. The corresponding inverse critical temperature L_c (in units of the lattice spacing) is given in second column. In the third column appear the corresponding minimal sizes used in MC simulations. In the last two columns we present estimates for the bulk correlation length from a Monte Carlo simulation and from an analysis of the low temperature series with inhomogeneous differential approximants [17].

L_1	L_2	ΔE	$\Delta E^{(\text{CWM})}$	x
13	13	0.04437(28)	0.04441	0.226
13	26	0.01657(28)	0.01682	0.181
13	30	0.01321(57)	0.01326	0.196
13	34	0.01069(40)	0.01059	0.217
14	14	0.03617(32)	0.03627	0.267
14	28	0.01157(62)	0.01156	0.156
14	32	0.00916(51)	0.00880	0.168
14	34	0.00723(65)	0.00771	0.176
16	16	0.02398(29)	0.02355	0.149
18	18	0.01451(46)	0.01468	0.118

Tab. 2. The energy gaps ΔE obtained at $\beta = 0.2246$ from MC simulations with the TSC method are reported together with the best fit values to the CWM at 2-loop approximation given by Eq. (37). In the last column the values of the two-loop parameter x defined in Eq. (66) are given.

L_1	L_2	ΔE	$\Delta E^{(CWM)}$	x
12	12	0.03750(23)	0.03765	0.184
12	24	0.01126(13)	0.01117	0.212
12	26	0.00939(13)	0.00940	0.154
12	28	0.00769(29)	0.00793	0.161
12	30	0.00665(21)	0.00672	0.170
13	26	0.00662(23)	0.00684	0.126
13	28	0.00554(32)	0.00562	0.130
14	14	0.02225(16)	0.02212	0.135
16	16	0.01236(45)	0.01222	0.104
18	18	0.00617(48)	0.00631	0.082

Tab. 3. *The same as Tab. 2, but for $\beta = 0.2258$.*

L_1	L_2	ΔE	$\Delta E^{(CWM)}$	x
10	10	0.04334(8) ^a	0.04335	0.265
10	18	0.01439(26) ^b	0.01457	0.131
10	20	0.01099(23) ^b	0.01148	0.136
10	23	0.00797(23) ^b	0.00813	0.147
10	26	0.00584(23) ^b	0.00583	0.162
10	28	0.00396(44) ^b	0.00469	0.174
10	32	0.00289(32) ^b	0.00307	0.200
11	30	0.00169(35)	0.00213	0.140
11	35	0.00114(38)	0.00113	0.164
12	12	0.0217(1) ^a	0.0217	0.118
12	15	0.01296(21) ^c	0.01274	0.099
14	14	0.00989(7) ^a	0.00979	0.087
14	18	0.00431(7) ^c	0.00432	0.071
16	16	0.00400(7) ^a	0.00397	0.066
18	18	0.00151(8) ^a	0.00144	0.052
20	20	0.000454(11) ^c	0.000466	0.042
24	24	0.000035(2) ^c	0.000034	0.029
26	26	0.000009(1) ^c	0.000008	0.025

Tab. 4. *The same as Tab. 2, but for $\beta = 0.2275$. The (a) and (b) are data taken from Ref. [27] and [4], respectively; the (c) data have been obtained with the BF method.*

L_1	L_2	t	ΔE	$\Delta E^{(CWM)}$	x
18	18	54	0.0230(2) ^a	0.0229	0.161
18	30	60	0.008628(95)	0.008650	0.124
18	35	70	0.005993(74)	0.006046	0.128
18	40	120	0.004242(42)	0.004289	0.137
18	45	90	0.003034(41)	0.003076	0.149
18	50	100	0.002214(35)	0.002224	0.164
20	30	80	0.006156(90)	0.006149	0.101
20	35	70	0.004010(72)	0.004021	0.101
20	40	80	0.002681(53)	0.002669	0.105
20	45	90	0.001810(39)	0.001790	0.112
20	50	150	0.001205(14)	0.001210	0.121
24	24	72	0.00657(8) ^a	0.00646	0.091
24	35	70	0.001925(32)	0.001885	0.071
24	40	80	0.001102(22)	0.001107	0.070
24	45	180	0.000652(11)	0.000657	0.071
24	50	100	0.000407(10)	0.000393	0.074
24	60	120	0.000145(5)	0.000143	0.084
30	30	90	0.00136(3) ^a	0.00133	0.058

Tab. 5. Data at $\beta = 0.2240$ obtained with the BF method, where the data with index (a) have been taken from Ref. [31]. The best fit values to Eq. (37) are given in the fourth column. The t -extensions of the lattices in the z -direction are also reported.

L_1	L_2	t	E_S	$E_S^{(CWM)}$	x
4	16	20	188.57(22)		0.40
5	20	30	348.49(22)		0.26
6	24	30,40	521.73(16)		0.18
7	28	40	720.90(28)		0.13
8	8	30	214.19(8)		0.07
8	32	30,40	949.58(18)		0.08
9	9	30	278.85(7)		0.05
9	16	20	518.58(17)		0.04
9	36	30,40	1207.47(17)		0.08
9	64	30	2173.99(53)		0.16
10	10	30	350.96(7)	351.06	0.04
10	40	30,40	1496.65(19)	1496.47	0.06
11	11	30	430.66(8)	430.62	0.03
11	44	30,40	1816.17(25)	1815.98	0.05
12	12	30,40	517.94(9)	517.93	0.03
12	48	40	2165.83(35)	2166.18	0.05
13	13	30	613.07(9)	612.95	0.02
14	14	30,40	715.73(17)	715.66	0.02
15	15	30	825.83(19)	826.04	0.02
16	16	30,40	944.16(18)	944.08	0.02
18	18	30,40	1203.11(15)	1203.12	0.01
20	20	30,40	1492.86(20)	1492.73	0.01
22	22	30,40	1812.86(21)	1812.89	0.009
24	24	30,40	2163.25(23)	2163.58	0.007

Tab. 6. *Data for the surface energy at $\beta = 0.240$ obtained by MC simulations with the local demon algorithm. The CWM best fit values of Eq. (37) to these data are given in the case $L_1 \geq 10$. In the last column the values of the two-loop parameter x defined in Eq. (66) are given.*

β	approx.	χ^2/dof	C.L.	dof	σ	$\lambda/\sqrt{\sigma}$
0.2240	2l	0.63	86%	16	0.004778(14)	1.343(13)
	1l	2.02	1 %	16	0.004839(14)	1.561(15)
	cl	66.0	0 %	16	0.004534(14)	1.480(13)
0.2246	2l	0.54	82%	8	0.006547(69)	1.354(16)
	1l	1.89	6 %	8	0.006792(69)	1.681(18)
	cl	17.5	0 %	8	0.005987(73)	1.539(16)
0.2258	2l	0.45	89%	8	0.009418(61)	1.271(14)
	1l	1.50	15%	8	0.009587(61)	1.511(15)
	cl	20.2	0 %	8	0.008363(63)	1.324(13)
0.2275	2l	1.05	40%	16	0.014728(40)	1.332(5)
	1l	2.36	0 %	16	0.015283(40)	1.612(6)
	cl	18.3	0 %	16	0.015114(39)	1.594(6)

Tab. 7. For each β , we report the best fit results obtained using Eq. (37), Eq. (18) and Eq. (19), which correspond to 2-loop, 1-loop and classical approximation, respectively.

scaling law	approx.	χ^2/dof	C.L.	dof	σ_∞	ν	$\lambda/\sqrt{\sigma}$
Eq. (45)	2l	0.86	74%	44	1.47(1)	0.629(1)	1.333(8)
	1l	0.94	56%	33	1.55(2)	0.633(1)	1.535(10)
Eq. (69)	2l	0.88	70%	44	1.32(1)	0.618(1)	1.331(8)
	1l	0.94	56%	33	1.38(1)	0.622(1)	1.533(10)

Tab. 8. Fits on the samples defined by Eq. (70), with $x_{cut} \approx 0.2$ and $x_{cut} \approx 0.15$ for the two-loop Eq. (68) and the one-loop Eq. (67), respectively.

scaling law	x_{av}	approx.	χ^2/dof	C.L.	dof	σ_∞	ν	$\lambda/\sqrt{\sigma}$
Eq. (45)	0.04	2l	1.39	25%	2	1.53(6)	0.636(7)	1.24(13)
		1l	1.50	22%	2	1.55(6)	0.637(7)	1.33(14)
	0.07	2l	0.65	66%	5	1.49(6)	0.630(3)	1.35(7)
		1l	0.72	61%	5	1.48(6)	0.630(3)	1.43(7)
	0.10	2l	0.24	95%	5	1.48(4)	0.629(2)	1.37(5)
		1l	0.35	88%	5	1.50(5)	0.631(2)	1.48(5)
	0.12	2l	0.78	54%	4	1.44(6)	0.627(4)	1.32(3)
		1l	0.82	51%	4	1.47(6)	0.629(4)	1.49(3)
	0.14	2l	1.31	25%	6	1.49(4)	0.630(3)	1.33(2)
		1l	1.96	7%	6	1.51(4)	0.631(3)	1.52(2)
	0.16	2l	0.78	59%	6	1.50(7)	0.630(5)	1.35(2)
		1l	0.74	62%	6	1.50(7)	0.630(5)	1.57(2)
	0.21	2l	2.87	1%	7	1.28(4)	0.612(3)	1.31(1)
		1l	6.16	0%	7	1.58(5)	0.634(4)	1.61(1)
Eq. (69)	0.04	2l	1.39	25%	2	1.37(5)	0.625(7)	1.24(13)
		1l	1.50	22%	2	1.39(5)	0.626(7)	1.33(14)
	0.07	2l	0.66	65%	5	1.33(5)	0.619(3)	1.35(7)
		1l	0.72	61%	5	1.33(5)	0.619(3)	1.43(7)
	0.10	2l	0.24	95%	5	1.33(4)	0.618(2)	1.37(5)
		1l	0.34	89%	5	1.34(5)	0.620(2)	1.48(5)
	0.12	2l	0.87	48%	4	1.29(5)	0.616(4)	1.32(3)
		1l	0.88	47%	4	1.32(5)	0.618(4)	1.49(3)
	0.14	2l	1.07	38%	6	1.34(4)	0.620(3)	1.33(2)
		1l	1.70	12%	6	1.35(4)	0.621(3)	1.51(2)
	0.16	2l	0.77	59%	6	1.35(6)	0.620(5)	1.35(2)
		1l	0.73	62%	6	1.35(6)	0.620(5)	1.57(2)
	0.21	2l	2.83	1%	7	1.14(3)	0.600(3)	1.31(1)
		1l	6.19	0%	7	1.40(4)	0.622(4)	1.61(1)

Tab. 9. *Fits on the samples defined by Eq. (71).*

L	ΔE_S	ΔE_S^{CWM}
8	-25.62(30)	21.754(159)
10	-2.47(29)	13.923(102)
12	3.79(25)	9.669(71)
14	5.17(45)	7.103(52)
16	5.42(36)	5.439(40)
18	4.36(32)	4.297(31)
20	3.79(39)	3.481(25)
22	3.31(46)	2.877(21)
24	2.58(58)	2.417(18)

Tab. 10. Differences of surface energies at $\beta = 0.240$, obtained from Eq. (74) with the data of Tab. 6 and the notation $L = 2L_1 = L_2/2$. The theoretical predictions $\Delta E_S^{(CWM)}$ are given by Eqs. (77,72,73).

$L_1 \geq$	χ_{11}^2/dof	χ^2/dof	C.L.	dof	σ	σ'	λ'/λ
8	107.2	8.02	0.00	17	0.0620(7)	3.81383(24)	33.10(8)
9	83.3	2.25	0.00	15	0.0593(8)	3.81321(25)	33.12(9)
10	48.5	0.96	0.48	11	0.0569(12)	3.81292(29)	33.17(13)
11	24.1	0.66	0.74	9	0.0565(18)	3.81261(36)	33.10(17)
12	8.4	0.57	0.78	7	0.0596(37)	3.81213(50)	32.83(27)
13	1.7	0.72	0.60	5	0.057(11)	3.8123(14)	32.95(87)

Tab. 11. Data of Tab. 6 are fitted using Eq. (78). For comparison, the reduced χ^2 's are reported of the fits on the same sample of data using Eq. (63).

$L_1 \geq$	σ	σ'	$\sigma'/(2\sigma)$	ν
Eq. (72,73)	0.0590(2)	3.813(2)	32.31(13)	0.593(2)
10	0.0569(12)	3.81292(29)	33.5(7)	0.615(13)
11	0.0565(18)	3.81261(36)	33.7(1.1)	0.619(20)

Tab. 12. The scaling ratio $\sigma'/(2\sigma)$ is evaluated according to Eq. (79), with $\nu \simeq 0.63$ for three estimates of σ and σ' . In the last column the corresponding estimates of ν , using Eq. (80), are given.

Figure Captions

Fig. 1. Histogram of the magnetization for a typical MC ensemble at $\beta = 0.2275$, with lattice sizes $L_1 = 20$, $L_2 = 23$ and $t = 120$.

Fig. 2. MC data and best fit curves obtained with the two-loop formula (37) plotted for different values of β versus the classical interface area $A = L_1 L_2$. From top to bottom, the first three lines correspond to $\beta = 0.2246$, the next three to $\beta = 0.2258$ and the last two to $\beta = 0.2275$. The values are also given in Tabs. 2, 3 and 4, respectively.

Fig. 3. The same as Fig. 2 but for $\beta = 0.2240$.

Fig. 4. χ^2/dof of the fits made with the one-loop Eq. (67) (empty circles) and two-loop Eq. (68) (full circles) on the samples defined by Eq. (70).

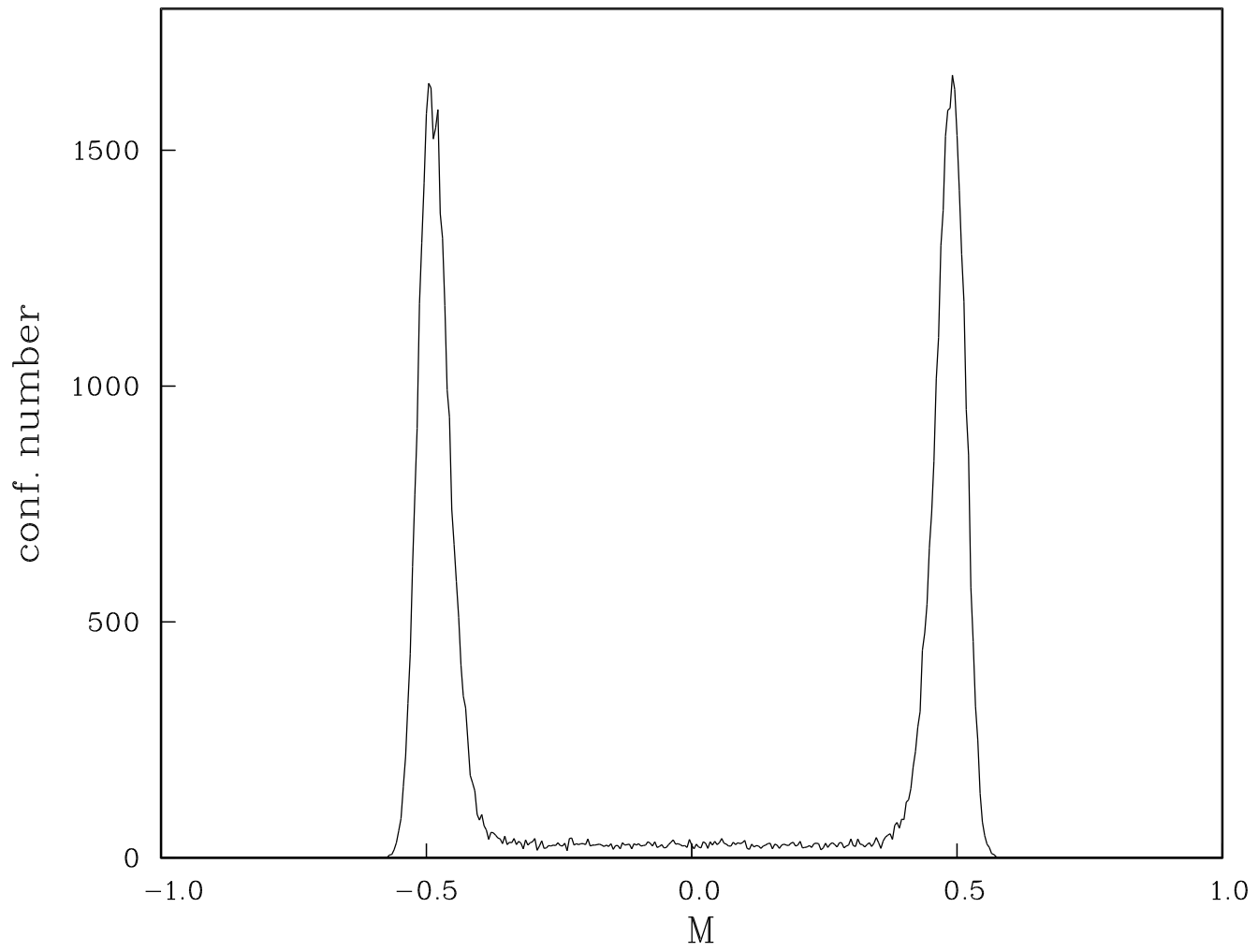
Fig. 5. Values of the constant $\lambda/\sqrt{\sigma}$ obtained fitting on the samples defined by Eq. (71) with the one-loop Eq. (67) (empty circles) and two-loop Eq. (68) (full circles).

Fig. 6. Comparison between Monte Carlo data and theoretical predictions (see Eq. (77) in the text) for the surface energy differences defined in Eq. (74). The corresponding values are also given in Tab. 10. The dotted line is the theoretical expectation if two-loop corrections are neglected.

This figure "fig1-1.png" is available in "png" format from:

<http://arxiv.org/ps/hep-lat/9407002v1>

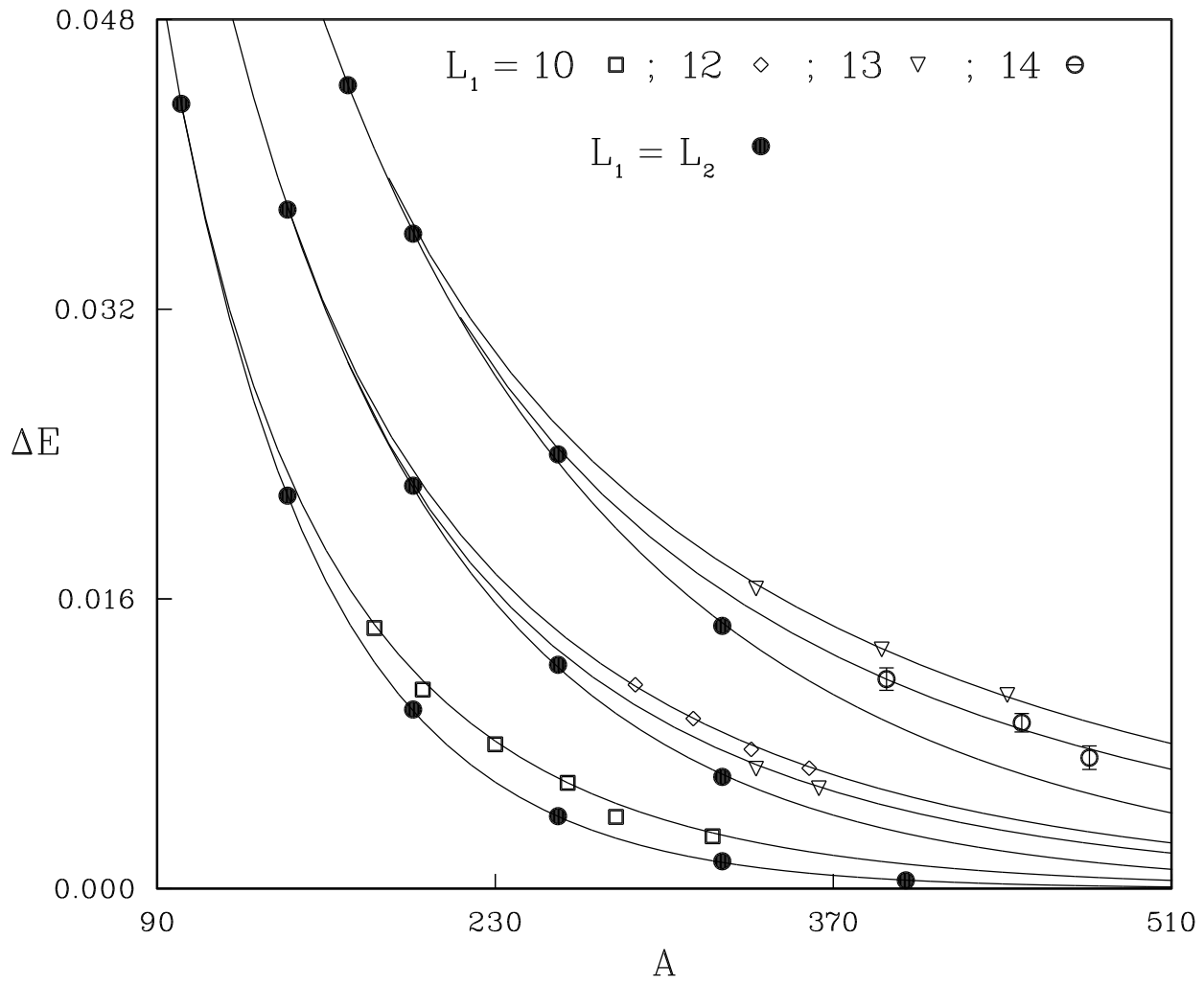
fig. 1



This figure "fig1-2.png" is available in "png" format from:

<http://arxiv.org/ps/hep-lat/9407002v1>

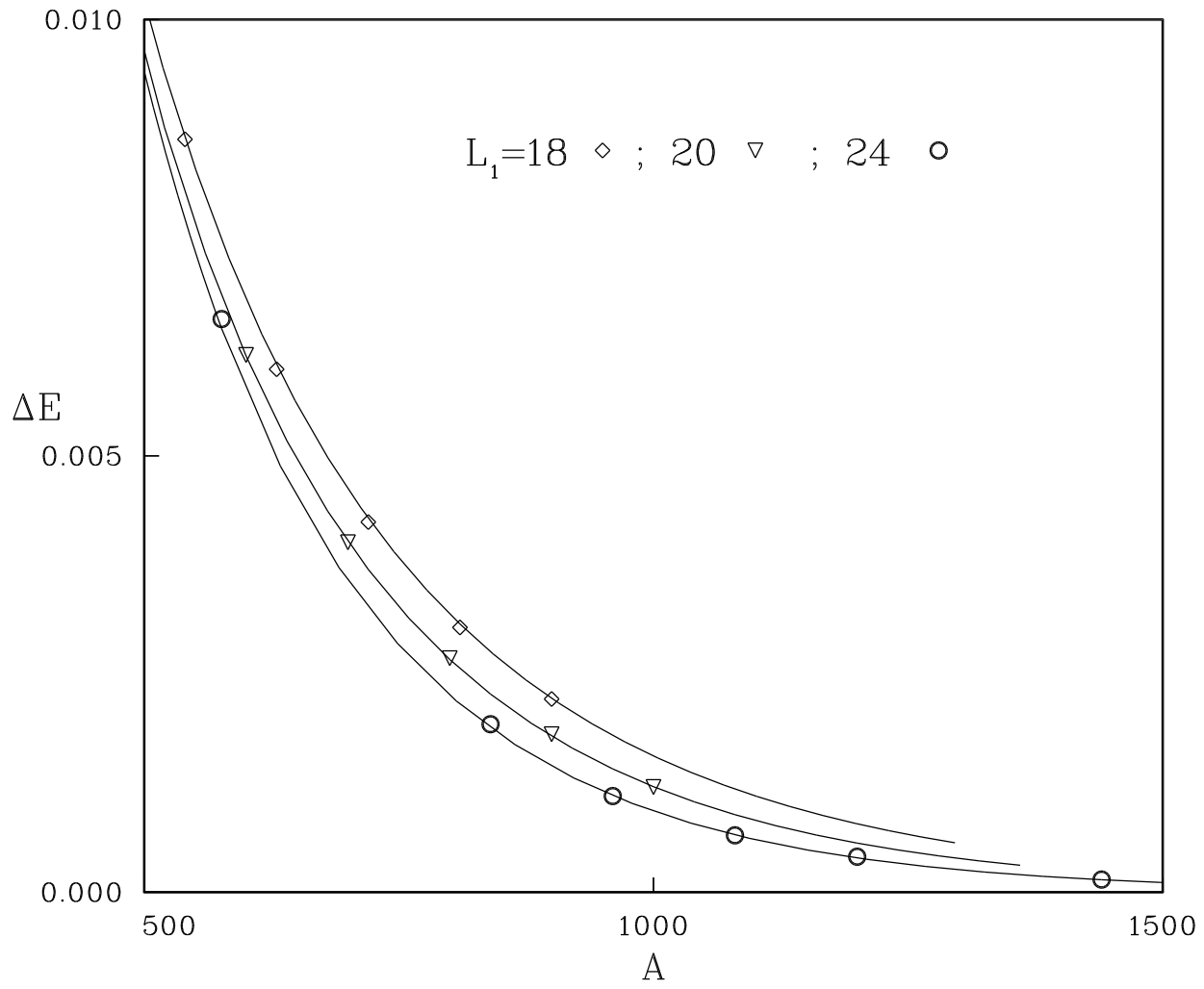
fig. 2



This figure "fig1-3.png" is available in "png" format from:

<http://arxiv.org/ps/hep-lat/9407002v1>

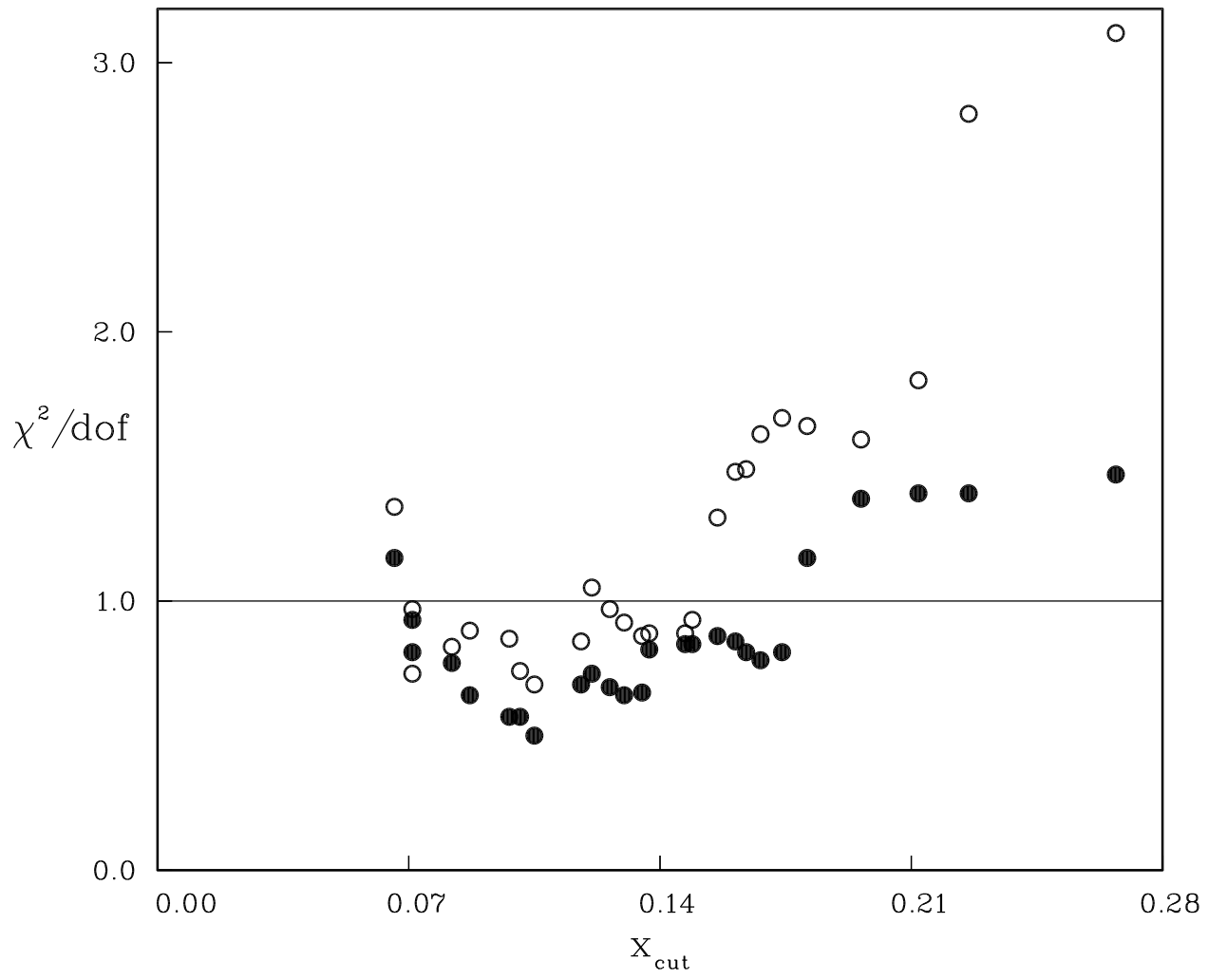
fig. 3



This figure "fig1-4.png" is available in "png" format from:

<http://arxiv.org/ps/hep-lat/9407002v1>

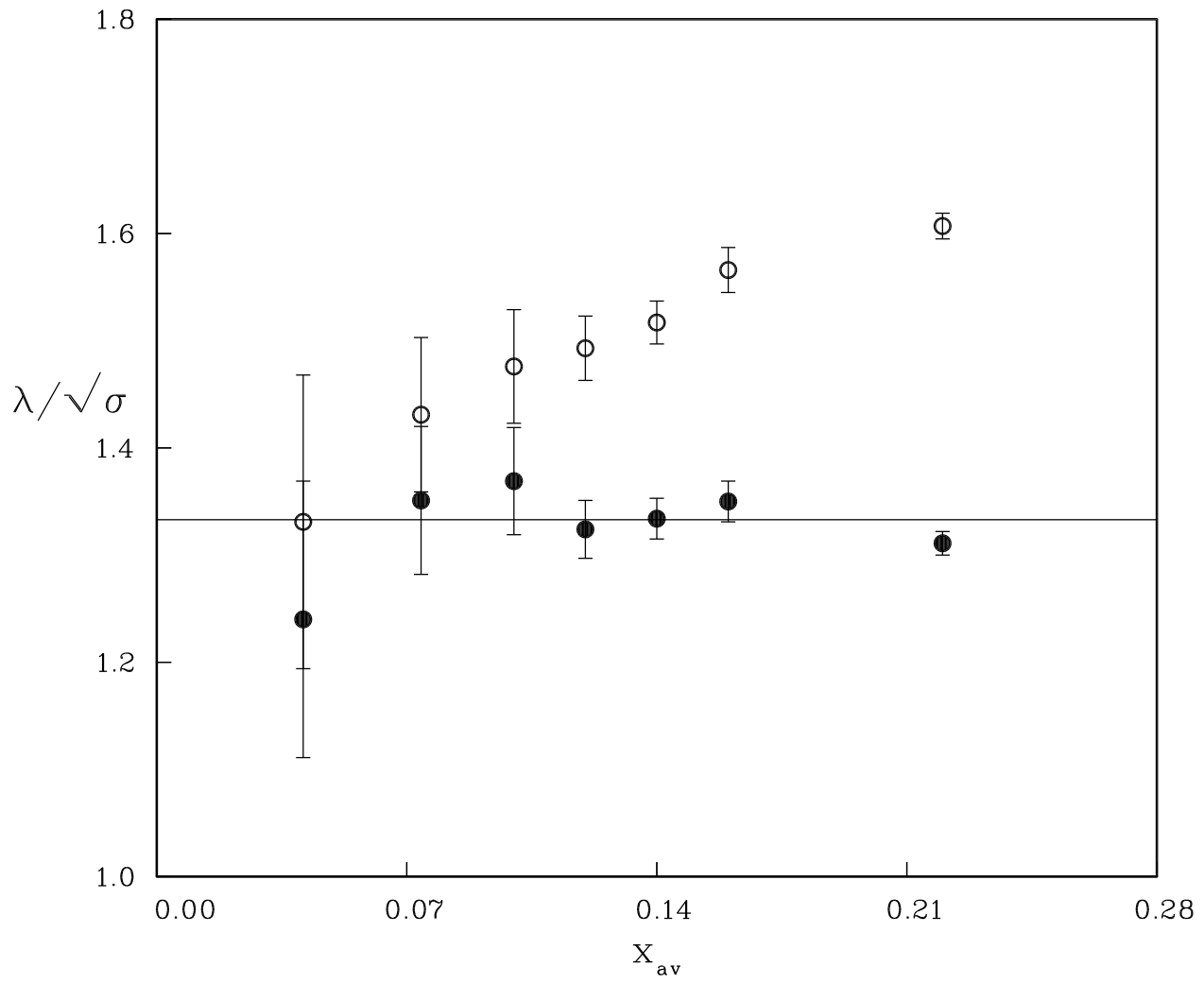
fig. 4



This figure "fig1-5.png" is available in "png" format from:

<http://arxiv.org/ps/hep-lat/9407002v1>

fig. 5



This figure "fig1-6.png" is available in "png" format from:

<http://arxiv.org/ps/hep-lat/9407002v1>

fig. 6

